Polymer Degradation and Stability 234 (2025) 111224

Contents lists available at ScienceDirect

Polymer Degradation and Stability

journal homepage: www.journals.elsevier.com/polymer-degradation-and-stability

Durability and performance of sustainable composite films from aliphatic-aromatic polyester with biomass-derived carbon-based filler particles

Nadka Tz. Dintcheva [a,*], Giulia Infurna [a], Antonio Messineo [b], Maurizio Volpe [b]

[a] Dipartimento di Ingegneria, Università degli Studi di Palermo, viale delle scienze Ed. 6, Palermo 90128, Italy
[b] Dipartimento di Ingegneria e Architettura, Università di Enna, Kore, Cittadella Universitaria, Enna 94100, Italy

ARTICLE INFO

Keywords:
Hydrothermal carbonisation
Slow pyrolysis
Hydrochar
Biochar
Poly(butylene adipate-co-terephthalate)
Bio-composites
Photo-oxidation behaviour

ABSTRACT

Additives are known to improve the properties of biopolymers, but most additives have environmental or performance concerns that limit their use. In this context, the recovery and use of bio-waste and biomass for the formulation of sustainable bio-composites is a challenging issue for the transition from a linear to a more sustainable circular economy. Recently, the replacement of carbon-based fillers in polymers and biopolymers with biochar particles derived from thermochemical treatments of biomass waste has attracted increasing attention for its potentially critical role.In this work, sustainable bio-composites based on biodegradable poly(butylene adipate-co-terephthalate), PBAT, and biochar, produced by controlled thermochemical treatments of biomass waste, were prepared by melt blending and their durability and performance were investigated in detail. Firstly, carob waste, after syrup extraction, was subjected to dry and wet thermochemical processes, *i.e.* slow pyrolysis at 280, 340 and 400 °C and hydrothermal carbonisation at 220, 250 and 280 °C, to obtain slow pyrolyzed biochar (SP-BC) and hydrothermal carbonised biochar (HTC-BC) particles. The SP-BC and HTC-BC, *i.e.* the solid phases resulting from the thermochemical processes, were characterised by elemental analysis and spectroscopy to study their physicochemical properties and by microscopy to analyse their morphology. Pure PBAT, PBAT/SP-BC and PBAT/HTC-BC bio-composites containing 10 % by weight of SP-BC and HTC-BC respectively were characterised by thermal, morphological, rheological and mechanical analyses. The results indicate that both types of particles exerted a reinforcing effect on PBAT and the resulting bio-composites were more thermo-mechanically stable compared to pure PBAT. Considering the potential application of these bio-composites as sustainable packaging materials, particular attention was paid to the photo-oxidation behaviour of these materials under accelerated artificial weathering conditions. Interestingly, both SP-BC and HTC-BC exerted a protective effect against the photooxidative ageing of PBAT, and this effect was more pronounced when HTC-BC was used.

1. Introduction

The transition from a linear to a circular economy requires the implementation of new approaches to how to produce, use and dispose of all goods and materials. It is necessary to understand and implement new real production pathways in relation to the efficient implementation of the "waste-to-materials" concept [1,2]. Therefore, the innovative design, production and end-of-life management of materials plays an important role in advancing the circular economy at the large-scale industrial level [3,4].

Furthermore, taking into account the new circular economy principles, many residual biomasses can be subjected to different thermochemical upgrading procedures to convert them into a high energy dense solid phase, commonly known as biochar together with variable amounts of gas and oily phases [5–9]. By varying the reaction conditions as temperature, rates, pressure, the presence of water and inert atmosphere, and nature of the starting material [10–13], the thermochemical treatments of biomasses could lead to the production of gases, oils and solid phases in different proportions [14]. It is well known that the solid phases, *i.e.* the biochar particles, are mainly composed of carbon atoms (up to about 90 %) and reduced amounts of hydrogen, nitrogen and oxygen atoms [15–18].

Therefore, producing biochar particles from biomass wastes offers a versatile and sustainable way to reuse biomass wastes, transforming

* Corresponding author.
E-mail address: nadka.dintcheva@unipa.it (N.Tz. Dintcheva).

https://doi.org/10.1016/j.polymdegradstab.2025.111224
Received 29 September 2024; Received in revised form 19 January 2025; Accepted 26 January 2025
Available online 27 January 2025

them into a resource. Interestingly, the biochar particles are proposed as useful resource for numerous applications, such as soil conditioners and pollutant [19], in animal farming [20], in the building sector [21–23], for waste water treatments [10,24,25], textiles, wellness [26,27], and recently, as CO_2 sequestrant agent [28–30]. Further applications of these sustainable particles need to be investigated and established to fully exploit their potentialities.

Hydrothermal carbonisation (HTC) of biomass is a thermochemical process that converts wet residual organic materials into a biochar at milder conditions, when compared to conventional pyrolysis [31–34]. The HTC process can successfully and efficiently convert various biomass feedstocks, such as agricultural residues, forest residues, organic municipal wastes, etc., in the presence of water (and thus without energetically expensive drying procedures) into a stable carbon-rich material called hydrochar (HTC-BC) [18,33,35]. During hydrothermal carbonisation, water acts as a solvent catalysing biomass degradation through a series of hydrolysis, dehydration and decarbonylation reactions where water promotes mass and heat transfer [36]. HTC-BC particles, like Slow Pyrolysis Biochar (SP-BC) particles, can potentially be used in a wide range of applications, from agriculture to environmental and soil pollution and remediation [18,19,35]. However, even if for some particular feedstock as sludges the scale-up at the industrial level is being successfully implemented, challenges remain in optimising and scale-up of the process for different feedstocks [37]. In this context, the formulation of sustainable bio-composites using biopolymers and naturally occurring additives, offers several potential environmental benefits such as reducing dependence on fossil resources, reducing carbon footprint, formulating materials with designed degradability and compostability, etc. Biopolymers with suitable properties for the formulation of high-performance bio-composites are polylactic acid (PLA), poly-butylene adipate terephthalate (PBAT), poly-butylene succinate (PBS), starch-based biopolymers, chitosan, pectic, etc. It is worth noting that the environmental impact of these biopolymers depends on the feedstock, production processes and end-of-life management, and other important issues such as production scalability, costs and "first-food" principle need to be addressed to ensure the transition towards sustainable and circular economy [32,37].

Currently, to formulate sustainable bio-composites, biopolymer-based matrices have been added with different carbon-rich particles derived from biomasses treated through carbonisation [18,35]. Based on this, the current work proposed the formulation and characterization of sustainable bio-composites by melt compounding based on poly-butylene adipate terephthalate (PBAT) and containing biochar particles produced by two different thermochemical methods, *i.e.*, slow pyrolysis (SP) and hydrothermal carbonisation (HTC). Biomass waste, specifically, carob waste after syrup extraction, was subjected to slow pyrolysis at three different temperatures, *i.e.*, at 280, 340 and 400 °C to produce biochar particles (SP-BC), and to hydrothermal carbonisation, at 220, 250 and 280 °C, to produce hydrochar particles (HTC-BC). The treatment temperatures were chosen taking into account prior thermogravimetric analysis to determine the maximum rates of mass loss (not shown here). Production yields at each temperature were analysed for both slow pyrolysis and hydrothermal carbonisation processes in terms of gas/oil/solids fractions. Both SP-BC and HTC-BC particles were subjected to accurate elemental analysis by CHN test, thermogravimetry, spectroscopy and morphological analysis. PBAT was then added at 10%wt. to each SP-BC and HTC-BC particles and the resulting formulated sustainable bio-composites were characterised by rheological analysis, tensile test, dynamic mechanical test and calorimetric analysis. Particular attention was paid to the durability under accelerated artificial weathering, considering the potential applications of these bio-composites in agricultural and packaging sectors.

2. Experimental part

2.1. Materials

Poly(butylene adipate-co-terephthalate), (PBAT), (commercial Ecoflex® F Blend C1200, BASF, SE, Ludwigshafen, Germany) is a film grade with a melt flow rate (MFR) of 2.7–4.9 g/10 min (190 °C, 2.16 kg), a density in the range of 1.25–1.27 g/cm^3 and a melting temperature in the range of 110–120 °C. Biochar particles (SP-BC) were produced from carob waste (after syrup extraction for candy production) employing slow pyrolysis for fuel production. The slow pyrolysis process is described in detail in our previous work [5]. The biochar particles are named SP-BC280, SP-BC340 and SP-BC400 as a result of pyrolysis at three different temperatures, *i.e.* 280, 340 and 400 °C. The choice of these heat treatment temperatures is linked to the possibility of maximising the lignin-cellulose content and preventing total carbonisation of the carob waste, according to our previous study [5].

Hydrochar particles (HTC-BC) were produced from carob waste (after syrup extraction for candy production) and used apparatus and processes are explained in depth in the following sub-paragraph 2.2. The hydrochar particles are named HTC-BC200, HTC-BC250 and HTC-BC280 as a result of hydrothermal carbonisation at three different temperatures, *i.e.* 220, 250 and 280 °C.

Residual pyrolyzed biochar and residual hydrochar from the two different thermochemical decompositions, considered in this work, were ground using a mechanical pestle and mortar for 60 min under the same process conditions. The diameters of both SP-BC and HTC-BC particles were *ca*. 150 ± 20 μm.

Scheme 1 shows the overall workflow and focus indicating the SP-BC and HTC-BC particle production, PBAT-based bio-composite production, durability, and performance characterisation. Further, images of carob waste feedstock, PBAT, PBAT/SP-BC and PBAT/HTC-BC samples and microscopy observations of both SP-BC and HCT-BC particles, are shown.

2.2. Thermochemical treatments of biowaste for the production of char particles

Carob waste was used as a raw material after the sugar extraction process to produce carob candy. As mentioned above, the SP-BC was produced considering three pyrolysis temperatures: 280, 340 and 400 °C, as well as HTC-BC at 220, 250 and 280 °C.

Slow pyrolysis (SP) was carried out as described in the previous paper [5]. Hydrothermal Carbonisation (HTC) runs were performed using a 500 mL internal volume, stirred (200 rpm) stainless steel batch reactor. For each experiment, to achieve a biomass to water ratio (B/M) of approximately 0.1, the reactor was charged with approximately 38.0 ± ± 0.5 g thawed carob waste (approximately 30.0 g feedstock on a dry basis d.b.) and approximately 300.0 ± ± 0.5 g deionised water (DW). After the reactor was filled with the feedstock and DW, it was sealed, evacuated and purged three times with pure nitrogen to remove residual traces of oxygen. After purging, the reactor was heated up to the selected temperature and maintained isothermally for the pre-determined reaction time of 1 h. (The heating step lasted 25–40 min, depending on the temperature set point.) The reaction temperatures and the corresponding reaction pressures were in the range of 220–280 °C and 20–60 bar, respectively. At the end of the reaction time, chilled (20 °C) water flowing through a cooling coil inside the reactor body was used to rapidly cool the reactor to room temperature. Prior to opening the reactor, the gaseous phase produced was passed through an outlet valve into a graduated cylinder filled with water, and its mass was evaluated using the ideal gas law, assuming atmospheric pressure, a temperature of 30 °C and CO_2 as the only gaseous product. It is well established in the HTC literature that CO_2 is the predominant gaseous product (often above 90 wt%), accompanied by small amounts of CO and light hydrocarbons [32]. The solid-liquid reaction mixture was separated using

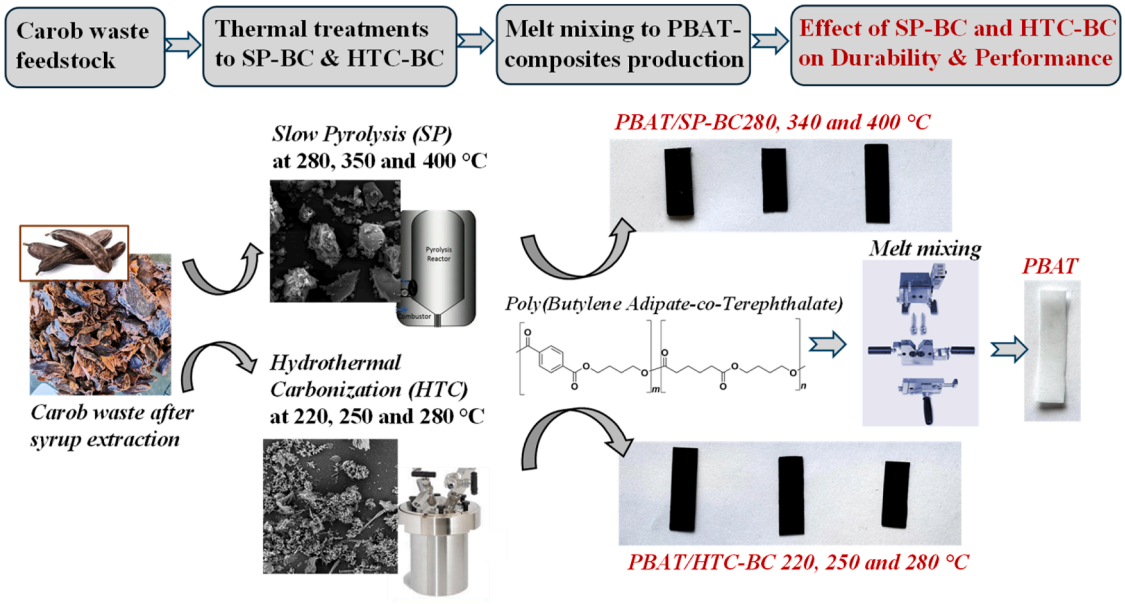

Scheme 1. The overall workflow and focus from SP-BC and HTC-BC particle production to PBAT composite durability and performance characterisation.

a vacuum filtration unit and a pre-weighed cellulose filter. The solid fraction in the filter was washed a few times with DW to remove the mother liquors, and the solid residue was dried in a ventilated oven at 55 °C until reaching a constant weight.

The hydrochar mass yield (MY_{HC}) and gas mass yield (MY_G) were evaluated through Eqs. (1) and (2) respectively, while liquid mass yield (MY_L) was calculated by difference through Eq. (3). M_{HC} and m_G are the mass of hydrochar (d.b.) and gas, collected after the conversion, respectively and mraw is the mass (d.b.) of the solid starting material.

$$MY_{HC} = m_{HC}/m_{raw} \quad (1)$$

$$MY_G = m_G/m_{raw} \quad (2)$$

$$MY_L = 1 - MY_{HC} - MY_G \quad (3)$$

The hydrochar energy properties were computed through the energy yield (EY) and the energy densification ratio (EDR), defined as follows:

$$EY = \frac{HHV_{HC}}{HHV_{raw}} \cdot MY_{HC} \quad (4)$$

$$EDR = \frac{HHV_{HC}}{HHV_{raw}} \quad (5)$$

where the HHV_{HC} and HHV_{raw} indicate the HHV values for the hydrochar and raw feedstock, respectively.

2.3. Characterization of carbon-based particles

Elemental analysis was carried out in a LECO CHN 828 series Elemental Analyzer to determine carbon (C), hydrogen (H) and nitrogen (N) contents. A calorimeter LECO AC500 was used to measure the High Heating Values, HHVs, according to the CEN/TS 14,918 standard. The microstructure of biochar particles obtained after pyrolysis treatment was investigated using a scanning electron microscope (SEM, Quanta 200 ESEM, FEI, Hillsboro, OR, USA). Prior to SEM analysis, biochar particles were sputtered (Scancoat Six Edwards, Crawley, UK), with a thin layer of gold under argon atmosphere for 90 s, in order to avoid electrostatic charging under electron beam. In order to characterize the carob waste and the resulting biochar and hydrochar, IR spectra were recorded using a Spectrum One (Perkin Elmer, Shelton, CT, USA) with eight scans at cm^{-1} resolution in the attenuated total reflectance (ATR) mode in the 4000-450 cm^{-1} range. Measurements were performed on both carob and the biochars produced at different operating conditions.

2.4. Formulation of PBAT-based bio-composites

Compounding of the bio-composites was carried out using a Brabender mixer at 170 °C with a mixing speed of 50 rpm for 5 min. Prior to compounding, PBAT, SP-BC and HTC-BC were dried at 60 °C overnight under vacuum to avoid hydrolysis during compounding. The six different particles, *i.e.* SP-BC280, SP-BC340, SP-BC400, HTC-BC200, HTC-BC250 and HTC-BC280, were added at 10%wt. into the PBAT matrix. The concentration of 10%wt. was chosen as a result of a good compromise between reinforcement actions of carbon-based particles and system morphology, *i.e.* efficient particles dispersion, also according to previous works [38,39]. Then the mixture was pelletised. The pure PBAT was subjected to the same processing conditions to be comparable with the bio-composites.

After drying for 24 h in a vacuum oven at 60 °C to avoid hydrolysis, thin films (about 200 μm thick) of pure PBAT and of all the bio-composites were obtained by compression moulding using a Carver Laboratory Press at a pressure of 1500 psi for 5 min at 170 °C.

2.5. Characterizations of bio-composites

Rheological tests were performed using a strain-controlled rheometer (ARES G2, TA Instrument, New Castle, DE, USA) in parallel plate geometry (plate diameter 25 mm). Frequency scans from 10^{-2} to 10^{2} rad/s were performed to measure complex viscosity (η*) and storage (G′) and loss (G″) moduli at the same processing temperatures. The strain amplitude was set at 5 %, which was found to be low enough to be in the linear viscoelastic regime in preliminary experiments with strain sweeps.

A scanning electron microscope (SEM, Quanta 200 ESEM, FEI, Hillsboro, OR, USA) was used to examine the microstructure of the bio-composites. Prior to the SEM analysis, the samples were fractured in liquid nitrogen. To avoid electrostatic charging under the electron beam, the fractured surface of each sample was sputtered (Scancoat Six Edwards, Crawley, UK) with a thin layer of gold for 90 s in an argon atmosphere.

The melting enthalpies of all samples were measured by DSC using a Shimadzu (Japan) DSC-60 instrument at a heating rate of 10 °C/min

from T ambient to 170 °C, as an average of five measurements. All samples of similar weight (~7 mg) were subjected to heating/cooling/heating and the thermal parameters were evaluated on the second heating scan, erasing the previous thermal history. The PBAT crystallinity, χc, was calculated using the equation:

$$\chi_c = \frac{\Delta H_m}{\Delta H_{100} - W_p} \times 100 \quad (6)$$

where ΔH_m is the enthalpy of fusion, ΔH_{100} is the enthalpy of fusion of 100 % crystalline polymer and W_p is the weight fraction of polymer. For PBAT ΔH_{100}=114 J g^{-1} [40].

Tensile tests were performed on rectangular specimens using a universal testing machine (Instron model 3365, UK) according to ASTM D882. The tests were performed at a tensile speed of 1 mm/min for 1 min to evaluate the Young's modulus, and then the speed was increased to 10 mm/min until the specimen broke. Average values were calculated for elongation at break, EB, modulus of elasticity, E, and tensile strength, TS.

A dynamic mechanical analyser model DMA +50 (Metravib, Limonest, France) was used to perform dynamic mechanical thermal tests (DMTA) in tensile configuration. The test was performed on three specimens ($w \times h$ = 10 mm×30 mm) of each composite from room temperature to 120 °C. The heating rate was 2 °C/min. For some composites, measuring was stopped before reaching 120 °C. The frequency was set at 1 Hz, and a prior static displacement of 2×10^{-5} m and a prior dynamic displacement of 10^{-5} m was set.

The gel content of the film samples was determined in accordance with the standardised ASTM D2765 method A, utilising tetrahydrofuran (THF) as the solvent [17]. For brevity, the test has been performed on PBAT/SP-BC280 and PBAT/HTC-BC280, before and after photo-oxidation treatment. The gel content was calculated using the following equation:

$$\%Extract = \frac{W_s - W_d}{f \cdot W_s} \times 100 = \frac{W_s - W_d}{(1-F) \cdot W_s} \times 100 \quad (7)$$

$$f = 1 - F = \frac{Total\ Sample\ Weight - Filler\ Weight}{Total\ Sample\ Weight} \quad (8)$$

$$\%Gel\ Content = 100 - \%Extract \quad (9)$$

In these equations, Ws represents the weight of the specimen undergoing testing, Wd denotes the weight of the dried gel, f signifies the polymer fraction, which is defined as the ratio of the weight of the polymer present in the formulation to the total weight of the formulation, and F is the fraction of filler.

2.6. Photo-oxidation behaviour

All samples were subjected to photo-oxidation again using a Q-UV/se accelerated weathering tester (Q-Labs Corp., Westlake, OH, USA) with eight UVB-313 lamps. The samples were exposed at 70 °C to an irradiance of 0.89 W/m^2 (at a wavelength of λ = 313 nm) and monitored every 24 h. ATR-FTIR spectroscopy and tensile test analyses monitored the progress of photo-oxidation in time of pure PBAT and all the PBAT-based bio-composites. Besides, the gel content on some films before (0 h) and after (96 h) the photo-oxidation was evaluated.

3. Results and discussion

3.1. Biochar particles characterization

To obtain biochar particles, the carob waste was subjected to thermochemical treatments through hydrothermal carbonization at three different temperatures, *i.e.* 220, 250 and 280 °C, and slow pyrolysis at three different operative temperatures, *i.e.* 280, 340 and 400 °C. Fig. 1 reports the products' yield for the two different thermochemical processes. It is worth noting that hydrothermal carbonisation results mainly in the formation of liquid and solid phases, and the production of the gas phase is minor at all temperatures considered, also according to the literature [31]. Therefore, for hydrothermal carbonisation, the data show that hydrocar mass yields progressively decrease down, with increasing temperature, to about 47%wt. at 280 °C with a concomitant increase of the liquid and gas yields being, at 280 °C, about 51 and 2.6% wt., respectively. The decrease of solid mass yields over 220 °C, in the presence of sub-critical water, has been related to the complete decomposition of cellulose and partial decomposition of the lignin fraction of starting biomass residues [41,42].

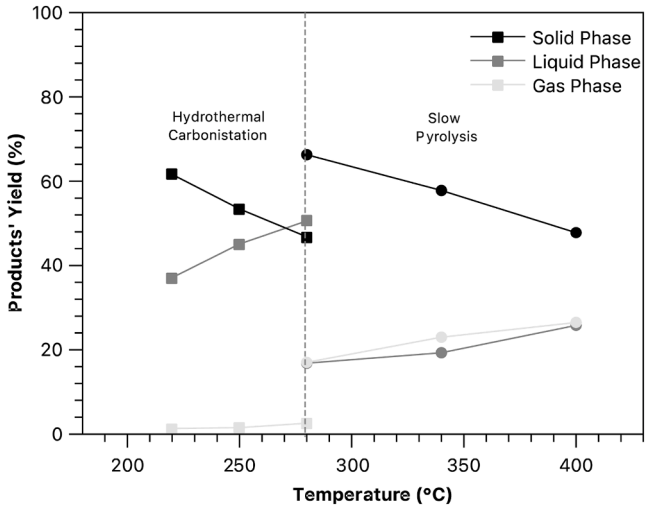

Fig. 1. Product yields at each temperature when carob was treated by hydrothermal carbonisation (square symbols) and slow pyrolysis (circle symbols).

The results of the products' yield for the slow pyrolysis reported in Fig. 1 highlights that the liquid phase yields increased with increasing temperature from 17%wt. at 280 °C to 27%wt. at 400 °C, and similar considerations could be made also for the produced gas fraction. The solid phase is the dominant fraction, and the mass yields decrease with increasing temperature from 67%wt. at 280 °C to 48%wt. at 400 °C, also according to the literature, this is a typical trend for slow biomass pyrolysis [6,7].

Interestingly, the two thermochemical treatments lead to the formation of solid phases with different yields from the same amount of biomass residues. In addition, as expected, the yield of the processes depends on the temperature of the treatment and the presence of water.

To explore the composition of the resulting particles, CHN elemental analysis was performed on the ground carob waste, SP-BC and HTC-BC particles, obtained at different temperatures. Table 1 reports the elemental composition (C, H and N contents) and High Heating Value (HHV) of the carob waste and resulting biochar.

The results show that the carbon content in SP-BC increases with

Table 1
Elemental Composition and High Heating Values (HHV) of carob waste, SP-BC (according to previous work [38]) and HTC-BC produced at different temperatures.

Sample	C [%]	H [%]	N [%]	HHV [MJ/Kg]
Carob Waste	46.94 ± ± 0.7	1.63 ± ± 0.04	5.44 ± ± 0.04	17.4
SP-BC 280	65.20 ± ± 0.2	1.75 ± ± 0.07	4.29 ± ± 0.02	23.5
SP-BC 340	68.90 ± ± 0.3	1.87 ± ± 0.09	3.79 ± ± 0.03	25.1
SP-BC 400	73.10 ± ± 0.2	2.09 ± ± 0.02	3.34 ± ± 0.06	28.6
HTC-BC 220	65.42 ± ± 0.3	2.21 ± 0.02	4.23 ± ± 0.06	22.7
HTC-BC 250	69.87 ± ± 0.3	2.23 ± ± 0.04	4.02 ± ± 0.07	24.8
HTC-BC 280	72.65 ± ± 0.3	2.25 ± ± 0.05	3.91 ± ± 0.07	26.7

increasing pyrolysis temperature, also according to the literature [8]. This is due to the carbonisation and thermochemical decomposition of the biomass that leads to carbon atoms enrichment. Thus, the structures of cellulose, hemicellulose and lignin are involved in a different resistant graphitic bond. It is worth emphasising that the enrichment of the particles with carbon atoms as a function of processing temperatures is accompanied by almost unchanged trends in hydrogen and nitrogen contents. The HHV of the solid fractions is the amount of heat released by the unit mass once it has been burned and the products have returned to a temperature of 25 °C (including the latent heat of water vaporisation). The HHVs of the SP-BC are 23.5, 25.1 and 28.6 MJ/kg at 280, 340 and 400 °C, respectively, showing, as expected, an increase with the increase of process temperature. Further, the HHVs of SP-BC are higher than the HHV of carob waste because of carbon enrichment upon slow pyrolysis treatment.

In the same way, and as commonly found in the literature, with the increasing temperature reaction, HTC-BC shows an increase in carbon content with an almost constant amount of hydrogen and nitrogen when compared to the starting material. This factor determines the final quality of biofuel due to the reactivity during combustion and the reduced possibility of slugging and fouling respectively [34,43]. Also in this process, the HHV of the HTC-BC increases as the operating temperature increases, up to 27.7 MJ/kg, showing the high potential of hydrochar as a biofuel in substitution or a mixture with standard coals. Elemental analysis confirms that the high heating value of HTC-BC is mainly driven by the increase in carbon content, which is directly dependent on the reaction temperature.

Fig. 2 the ATR-FTIR spectra of the carob waste, SP-BC and HTC-BC obtained at the three different process temperatures are shown. The ATR-FTIR spectrum of carob waste shows a broad band between 3300 and 3600 cm^{-1} due to ν_{OH}, and the signals of the peaks related to symmetric and asymmetric vibration of CH groups, *i.e.* 2930 and 2850 cm^{-1}. Additionally, the carob waste shows the two peaks usually attributed to the presence of carbonyl functions $\nu_{C=O}$ (1732 cm^{-1}) and unsaturation $\nu_{C=C}$ between 1680 and 1480 cm^{-1}.

For the pyrolysis process the broad band between 3300 and 3600 cm^{-1} due to ν_{OH}, decreases significantly for SP-BC280 and even more for SP-BC340 and SP-BC400, see Fig. 2. The signals of the peaks related to symmetric and asymmetric vibration of CH group, *i.e.* 2930 and 2850 cm^{-1} start to disappear, with no comparison for SP-BC340, the temperature at which the maximum degradation rate of hemicellulose occurs, and are no longer detected SP-BC400, probably due to the complete degradation of the hemicellulose biomass macro-component in this sample. Additionally, after the pyrolysis process, the peaks relative to $\nu_{C=O}$, at the highest temperature disappear, while the peaks relative to $\nu_{C=C}$ between 1680 and 1480 cm^{-1}, reduce in amplitude without

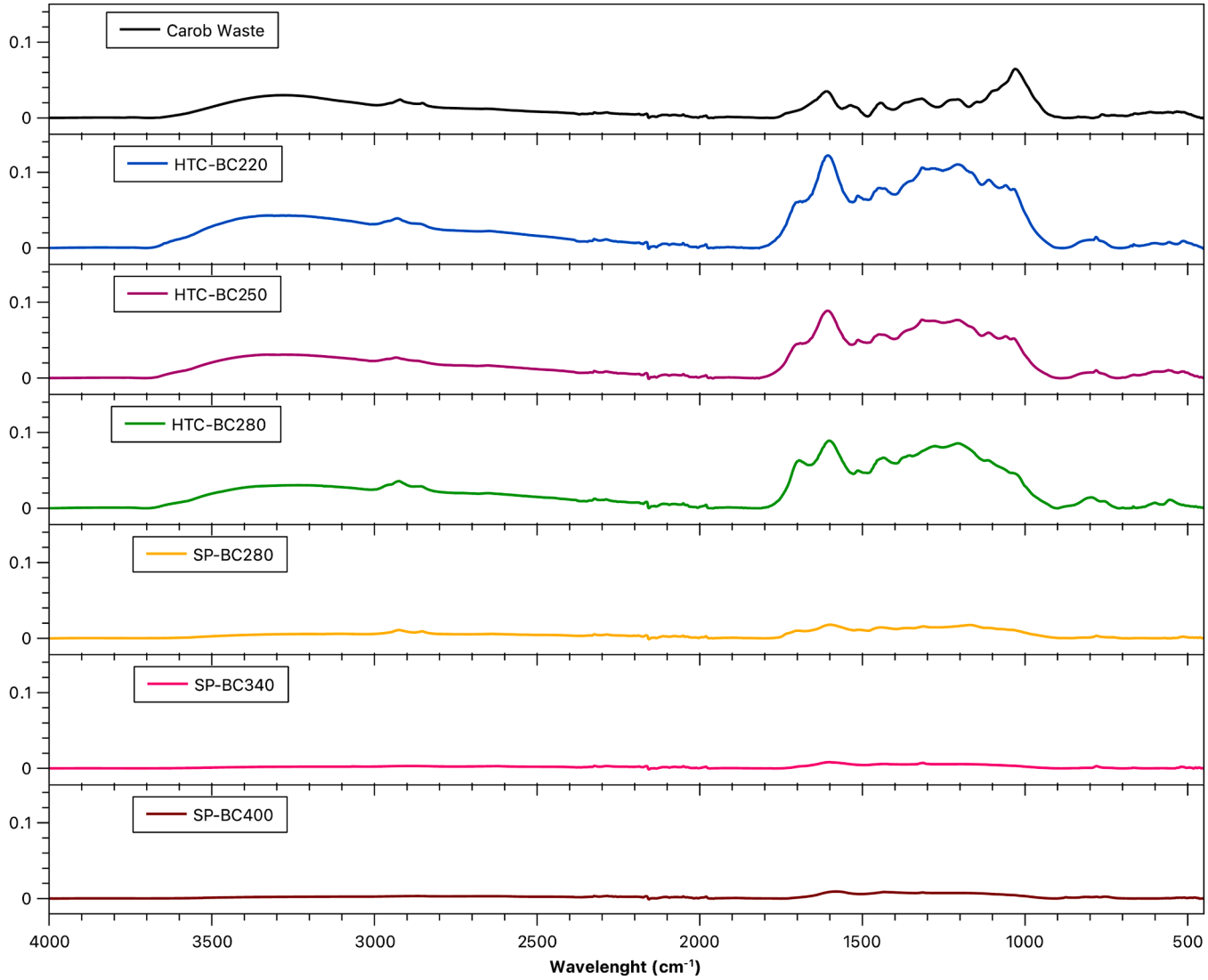

Fig. 2. ATR-FTIR spectra of carob waste and corresponding SP-BC [5] and carob waste and corresponding HTC-BC.

disappearing. This is because lignin degradation occurs at a higher temperature. Thus, the predominant functional group related to the hemicellulose structure and part of the lignin structure are lost as the temperature increases for the pyrolysis process.

About the hydrothermal carbonisation, the resulting ATR-FTIR spectra of HTC-BC as a function of operative temperature are shown in Fig. 2. For HTC-BC the broad bands between 3300 and 3600 cm^{-1} are preserved showing the presence of residual OH groups on the surface, probably due to their higher hydrophilicity. For HTC-BC, also the peaks related to sym and asym $\nu_{C\text{-}H}$ are preserved. The peak relative to $\nu_{C=O}$ significantly increases in comparison to carob waste, and the peaks relative to $\nu_{C=C}$, not only do not disappear but increase their amplitude. Being under decomposition temperature of cellulose, hemicellulose and lignin, probably the water molecules cause the reorganization of biomasses up to formation of larger amount of carbonyl function. Probably in this way, large number of chemical components present in the biomass rearrange themself, without any decomposition.

Fig. 3 shows the micrographs of the particles obtained by slow pyrolysis (a–c) and by hydrothermal carbonisation (d–f). The micrograph of SP-BC280 shows a typical lignocellulosic structure, whereas the micrograph of SP-BC400, as the pyrolysis temperature increases, appears more like a carbonaceous particle, more compact and less porous. On the other hand, the particles obtained by hydrothermal carbonisation have a sponge-like morphology, with high irregularity, regardless of the temperature at which they were obtained.

The SP-BC particles, regardless of the processing temperature, show an absence of aromatic structures and water molecules, appearing as lignocellulosic structures and easily recognized as typical fibrous structures commonly found in this kind of organic substrates, also according to the literature [44]. As discussed earlier, the HTC-BC particles contain higher amounts of aromatic structures and water molecules and seem much less regular. However, as known, the hydrochars derived from lignocellulosic biomasses commonly show an increase in surface area and porosity when compared to the starting raw material due to the partial release of volatile compounds during the treatments [45,46]. Although the two heat treatments, *i.e.* SP and HTC, result in the formation of carbon-rich particles and all of these particles were introduced into the chosen polymer matrix, for the sake of comparison, studies on the degradative effect were only conducted with particles produced at the same temperature.

3.2. Bio-composite characterizations

Oscillatory measurements were used to evaluate the rheological behaviour of all PBAT-based bio-composites in comparison to pure PBAT. The complex viscosity, storage modulus and loss modulus trends as a function of frequency for all PBAT-based composites are shown in Fig. 4a–c, respectively. For neat PBAT, a Newtonian behaviour of the sample is shown and the addition of 10 wt% BC particles to the PBAT matrix seems to preserve this behaviour. In addition, a slight increase in complex viscosity is observed with the addition of SP-BC, which is slightly pronounced at low frequency. The increases in viscosity from the addition of SP-BC appear to be minimal and no substantial difference is detected when considering the addition of particles produced at different temperatures, *i.e.* 280, 340 and 400 °C.

As far as biocomposite filled with 10 wt.% HTC-BC is concerned, the increase in complex viscosity is more pronounced and with HTC-BC obtained at lower hydrothermal carbonisation temperature (HTC-BC200) the highest complex viscosity is observed with the appearance of stress yield behaviour. Further, the trends of storage (G') and loss (G'') moduli, see Fig. 4b-c. The trends of both G' and G'' moduli, especially at low frequencies, show a noticeable stress yield behaviour.

However, the presence of SP-BC filler merely causes a vertical shift of the complex viscosity curve towards higher values, without actually modifying the rheological behaviour of the PBAT macromolecules. This behaviour is usually observed in polymer-based composites characterised by a low level of polymer-filler interaction, where the embedded particles are not able to significantly modify the dynamics of the macromolecules, but the particles exert only reinforcement action [47]. As a result, the dispersed SP-BC particles do not induce significant rheological change, and the rheological response of the bio-composites is governed by the rheological behaviour of the matrix.

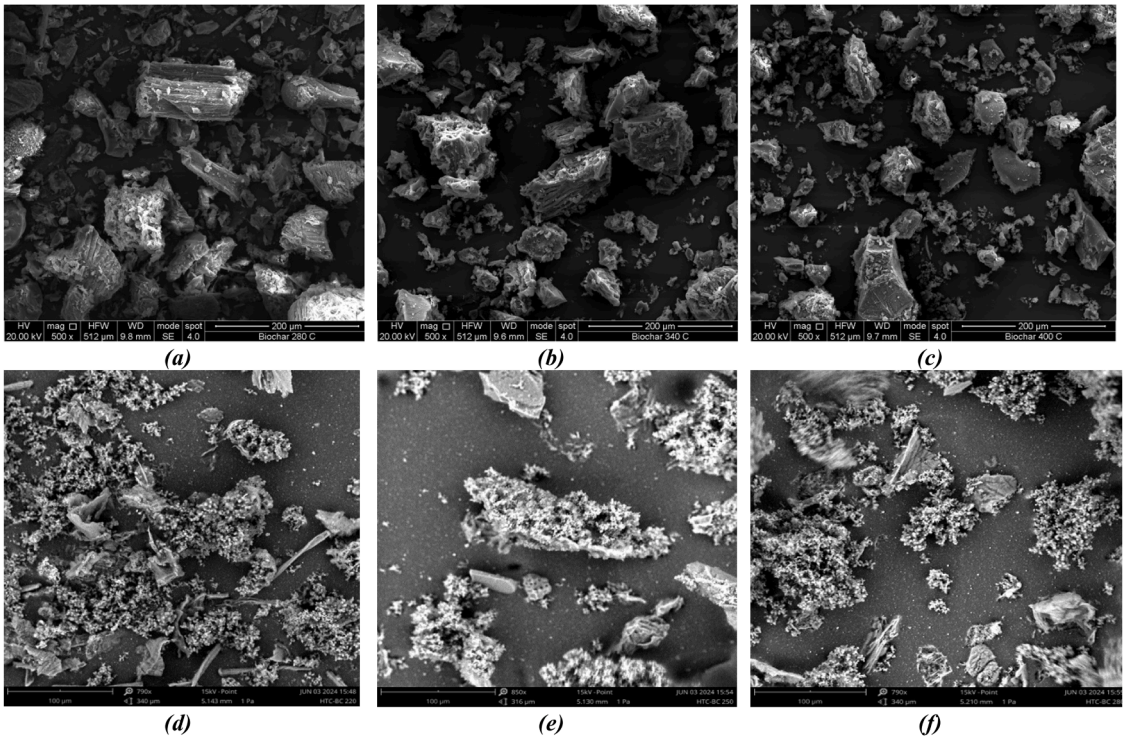

Fig. 3. SEM morphologies of (a) SP-BC280, (b) SP-BC340 and (c) SP-BC400 (d) HTC-BC200 (e) HTC-BC250 and (f) HTC-BC280.

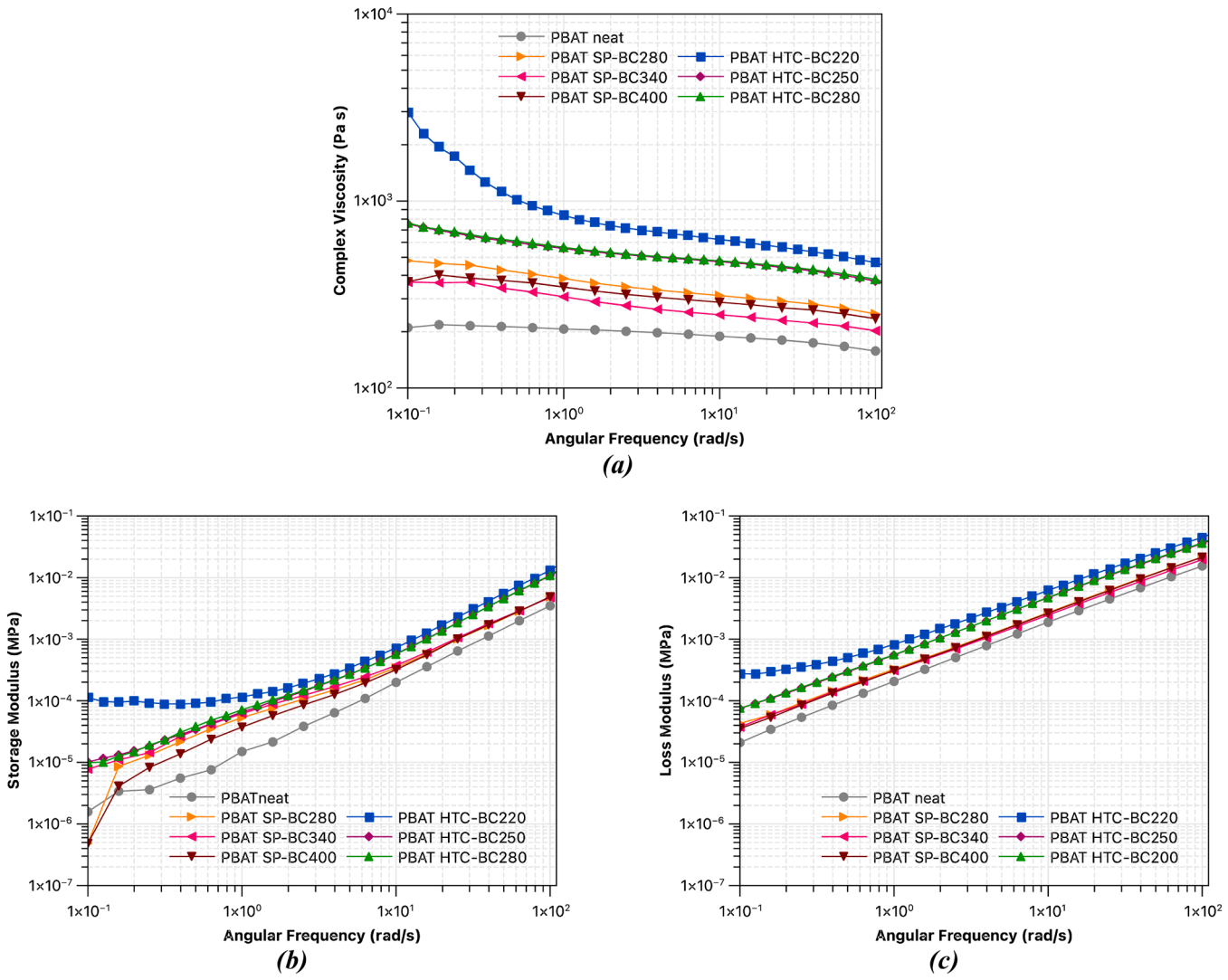

Fig. 4. (a) Complex Viscosity (b) Storage Modulus (G') and (c) Loss Modulus (G'') of pure PBAT and all the PBAT-based bio-composites.

Instead, the presence of HTC-BC causes a limitation in the relaxation of the macromolecules due to the restriction of chain motions as a result of the establishment of strong polymer-filler or filler-filler interactions [48]. In the case of HTC-BC containing bio-composites, it can be concluded that as the hydrothermal carbonisation temperature decreases, a slowing down of the PBAT chain mobility occurs due to some interactions between the polymer matrix and the embedded fillers. Moreover, the well pronounced yield stress for the sample PBAT/HTC-BC220 could be understood considering that at lower hydrothermal carbonisation temperatures, the particles contain large amounts of functional groups, also in accordance with above discussed analyses, that could promote the filler-polymer interaction, resulting in a change of rheological behaviour, *i.e.* significant viscosity and both moduli G' and G'' increases, especially in the low frequency range.

Fig. 5 represents the morphologies of the nitrogen fractures surface of PBAT/SP-BC and PBAT/HTC-BC bio-composites as a function of operative temperatures. The morphology of the fractured surface of all PBAT/SP-BC and PBAT/HTC-BC bio-composites suggests a good matrix-filler interfacial adhesion in all systems and this can probably be attributed to the affinity between the PBAT matrix and the fillers. Further, Fig. 5a shows a large SP-BC280 particle partially covered by PBAT, confirming that adhesion occurs between these particles and the matrix. It is noteworthy that the adhesion does not depend on the kind of employed thermo-degradation processes, and their operative temperatures.

Fig. 6 shows the DSC thermograms recorded during the second heating scan for all samples, comparing the PBAT SP-BC and PBAT HTC-BC composites with virgin PBAT; the resulting main characteristics of the cooling step and the second heating scan are listed in Table 2. Regarding the crystallisation temperature during the cooling scan, a different contribution of the two types of particles was highlighted. In fact, the addition of SP-BC led to a slight increase in T_c as the pyrolysis temperature increased. On the other hand, the addition of HTC-BC led to a decrease in T_c of 10 °C for SP-BC. For what concerns the melting temperature during the second heating scan, it highlights a slight increase in presence of SP-BC, that results more pronounced as the increase of pyrolysis temperature at which the particles have been obtained. Instead, when HTC-BC has been added to the PBAT matrix, T_m results almost constant except for PBAT/HTC-BC280 which results about 4 °C lower than the pristine PBAT. As a result of all these evaluations, it appears that the degree of crystallinity undergoes small but insignificant changes when SP-BC is added to the matrix, whereas the addition of HTC BC280 to PBAT resulted in a slight increase (about 2 %) in crystallinity.

However, as expected, the thermal behaviour, *i.e.* the transition temperatures Tc and Tm, depends on several factors, such as the heterogeneity of the system, the dispersion and distribution of the particles, and the interaction between the host matrix and the particles, which are

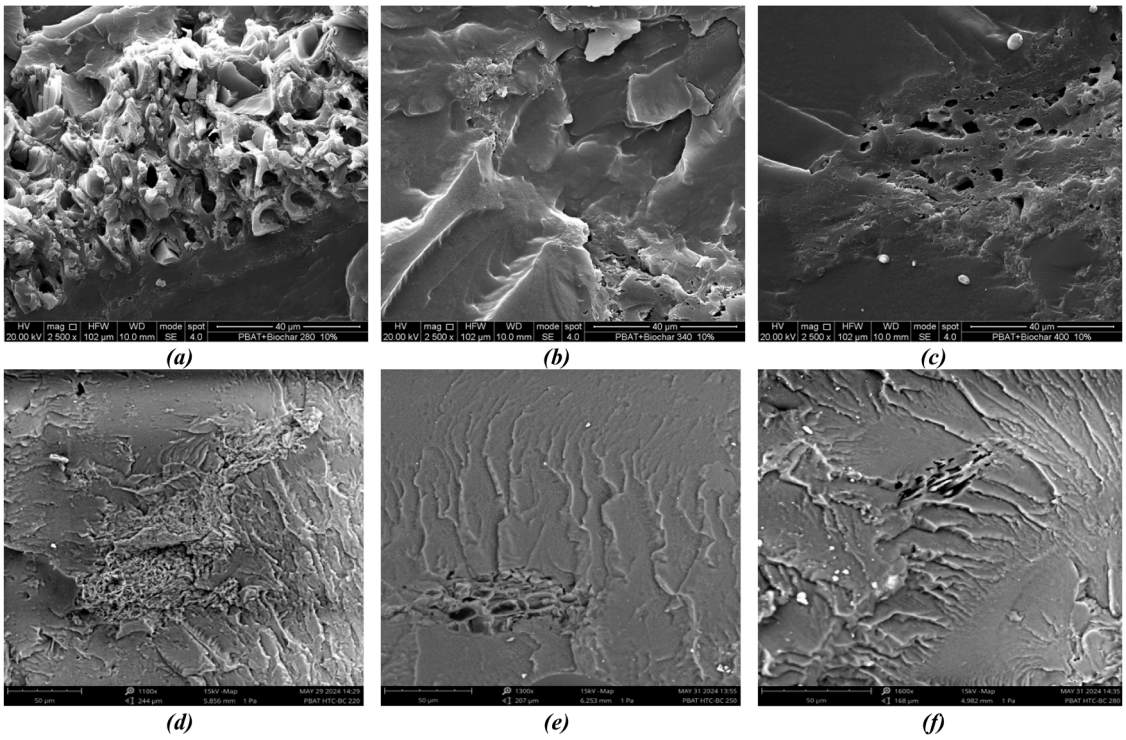

Fig. 5. SEM, micrographs of (a–c) PBAT/SP-BC 280-340-400 and (d–f) PBAT/HTC-BC 220-250-280 bio-composites as a function of operative temperatures.

significantly influenced by the functional groups presented, etc., and all this does not allow to identify a clear correlation between the transition temperature trends and the temperatures considered for the thermal treatments of the particles.

The mechanical properties of the PBAT-based composites were evaluated by tensile test and dynamical mechanical analysis. The main mechanical properties obtained by the tensile test are shown in Table 3. With increasing and pyrolysis temperature, the tensile values, *i.e.* E and TS, increase. As expected, the ductile behaviour of PBAT changes to a rigid behaviour with the addition of carbonaceous particles. Instead, the addition of HTC-BC greatly increases the stiffness of the final composites without the properties actually being affected by the increase in hydrothermal carbonisation temperature. It's worth noting that the effect of HTC-BC particles on the Young Modulus is in totally agreement with the trend observed in rheological analysis. Further confirmation of this, comes also by dynamical mechanical analysis. The storage modulus curves, E', of all the composites studied are shown as a function of temperature in Fig. 7.

The storage modulus at low temperature increases with increasing of pyrolysis temperature, following the same trend as the modulus of elasticity. The highest value of E' is obtained when HTC-BC is added to the PBAT matrix. Furthermore, E' decreases with increasing temperature for all samples. However, the presence of particles influences the softening temperature of the samples. Again, the trend is not influenced by the increase in the hydrothermal carbonisation temperature, even if at 80 °C the E' for both PBAT SP-BC and PBAT HTC-BC composites are significantly higher than the E' values of neat PBAT. It's worth noting that over 80 °C neat PBAT becomes rubber, while this change for both PBAT/SP-BC and PBAT/HTC-BC composites occurs over 100 °C.

3.3. Photo-oxidation behaviour of PBAT-based bio-composites

A Q-UV/SE accelerated weathering tester was used to subject all films to a photo-oxidation process, and the progress of photo-degradation in time of all investigated samples was monitored through ATR-FTIR spectroscopy analysis on the irradiated surface and tensile tests, collecting the samples every 24 h. Fig. 8a shows the ATR-FTIR spectra of pure PBAT at different exposure times and the insets correspond to a zoom on the wavelengths 3700-2700 cm^{-1} and 1850-1550 cm^{-1}, which are critical regions for highlighting the chemical modification that occurred during the photooxidative degradation. Fig. 8b reports the main degradation pathways followed by pure PBAT, which occur mainly by Norrish I and Norrish II reactions, according to the literature [49].

The spectrum of pure PBAT (0 h) shows different typical absorbance bands that are *(i)* broad band between 3700 and 3100 cm^{-1} assigned to the -OH vibrations; *(ii)* peaks at 2857 and 2874 cm^{-1} recognizable to the symmetric and antisymmetric CH_2 stretching; *(iii)* strong peak at 1710 cm^{-1} related to the symmetric stretching vibration of carbonyl groups, more specifically aliphatic C=O [50]; *(iv)* sharp peak at 720 cm^{-1} representing the CH_2 groups; *(v)* peaks around 1275-1250 cm^{-1} due to the C-O bond in the ester linkage [51,52]. Therefore, as expected, all these signals are significantly affected by the occurrence of the photo-oxidation phenomena, changing their intensity (*i.e.* height and/or width of the peaks) as a function of the exposure time. In

Fig. 8a, the photodegradation process of pure PBAT has been shown by means of recorded spectra and a significant reduction and broadening of the peak at 1710 cm^{-1}, relative to symmetric stretching vibration of C=O, is noticeable . In fact, according to the literature [49], the left shoulder (1790-1750 cm^{-1}) suggests the formation of free C=O and the right shoulder (1630-1590 cm^{-1}) represents the formation of a lower molecular weight ester. However, the degradation phenomena of pure PBAT occur mainly by the chain scissions following the Norrish I and II reactions, as schematically reported in Fig. 8b [49].

Therefore, according to the literature, the decrease/ disappearance of the peak at 1710 cm^{-1} can be related to the biodegradation (bio-erosion) of PBAT films by burial in soil [50] or PBAT modification and functionalisation [53]. Furthermore, an interesting computational study on the mechanism of CO_2 production during photo-oxidative degradation of PBAT showed the differences between the PBA and PBT segments considering oxygen-free and oxygen-rich conditions. However, the results show that UV radiation promotes the decarboxylation of the PBT segment as well as the oxidation and decomposition of the PBA segment

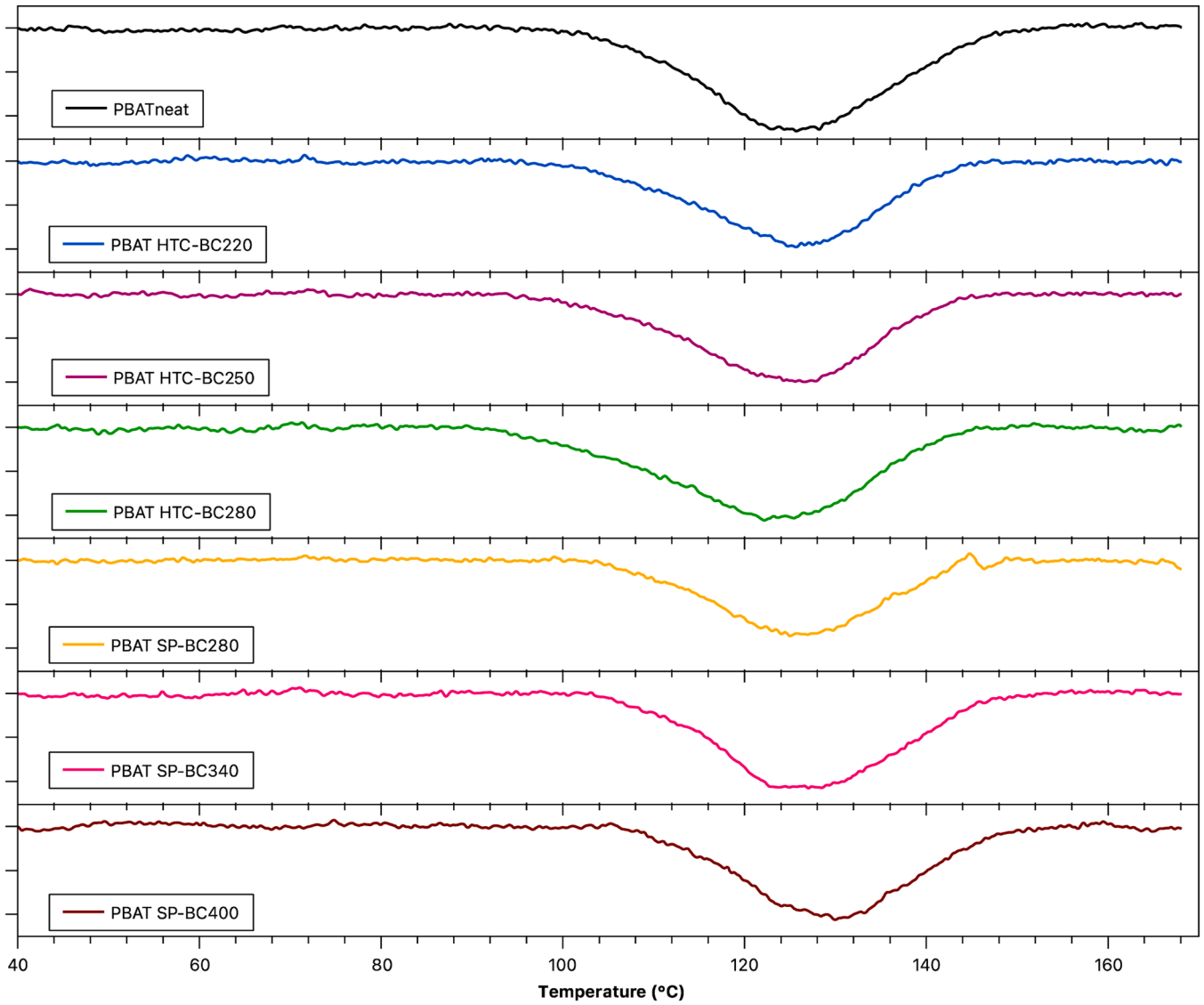

Fig. 6. Second heating scan of neat PBAT and all PBAT-based bio-composite filled with pyrolyzed and hydrothermal carbonised biomass.

Table 2
Main thermal properties collected during the cooling scan and the second heating scan and calculated crystalline degree for all investigated samples.

Sample	ΔH_c [J/gr]	T_c [°C]	$T_{c,\ onset}$ [°C]	$T_{c,\ offset}$ [°C]	ΔH_m [J/gr]	T_m [°C]	$T_{m,\ onset}$ [°C]	$T_{m,\ offset}$ [°C]	χ [%]
PBAT	−22.4	92.0	104.0	85.6	12.9	125.7	113.8	134.7	11.3
PBAT/SP-BC280	−19.3	93.1	103.1	86.1	10.7	124.1	107.2	136.8	10.4
PBAT/SP-BC340	−20.0	94.2	104.7	86.5	11.7	126.0	112.4	140.0	11.4
PBAT/SP-BC400	−17.5	94.5	103.8	88.0	12.7	127.2	112.9	141.6	12.4
PBAT/HTC-BC220	−19.3	92.4	101.9	84.4	11.6	125.0	114.9	139.1	11.3
PBAT/HTC-BC250	−15.2	90.5	99.9	83.6	9.8	126.8	113.5	137.6	9.5
PBAT/HTC-BC280	−20.3	82.0	91.0	76.1	14.0	121.3	109.6	140.5	13.6

with a synergy between UV radiation and oxygen [54]. The paper summarises that under oxygen-rich and UV conditions, there is no difference in the progress of degradation phenomena between PBA and PBT segments. The main differences in degradation pathways between the PBA and PBT segments are observed when UV exposure is performed under oxygen-free conditions.It seems that both SP-BC and HTC-BC have a pronounced effect not only on PBAT's strength and rheology, but also on its resistance to photo-oxidation. Specifically, all ATR-FTIR spectra of pure PBAT, PBAT/SP-BC (at 280, 340, 400 °C) and PBAT/HTC-BC (at 220, 250, 280 °C) films are reposted as supplementary figures (see Figs. S1–S7), and in Figs. 9 and 10, the peak at 1710 cm^{-1} and bands between 3700 and 2800 cm^{-1} of all the investigated samples are shown, respectively.

Firstly, when comparing the spectra of the bio-composites with pure PBAT, no significant peak shifts are visible, indicating that there are no chemical reactions between the particles and the matrix as a result of processing. Indeed, in the spectra of the bio-composites, the same typical bands of PBAT are found and all these signals tend to change their intensity as a function of UVB irradiation time, highlighting that photodegradation of the PBAT matrix is taking place. Interestingly, it seems

Table 3
Young Modulus (E), Tensile Strength (TS) and Elongation at Break (EB) of neat PBAT and PBAT-based composites.

Samples	Young Modulus [MPa]	Tensile Strength [MPa]	Elongation at Break [%]
PBAT	41.35 ± 0.58	9.35 ± 0.48	562.40 ± 152.6
PBAT/SP-BC280	50.09 ± 3.65	3.00 ± 0.72	16.08 ± 4.35
PBAT/SP-BC340	52.24 ± 4.17	4.08 ± 0.22	22.11 ± 2.16
PBAT/SP-BC400	65.05 ± 6.03	6.12 ± 0.76	31.10 ± 5.50
PBAT/HTC-BC220	83.23 ± 3.66	6.35 ± 0.68	22.57 ± 4.36
PBAT/HTC-BCC250	75.13 ± 4.55	6.88 ± 0.67	40.08 ± 12.33
PBAT/HTC-BC280	81.61 ± 3.20	7.72 ± 0.68	40.91 ± 8.68

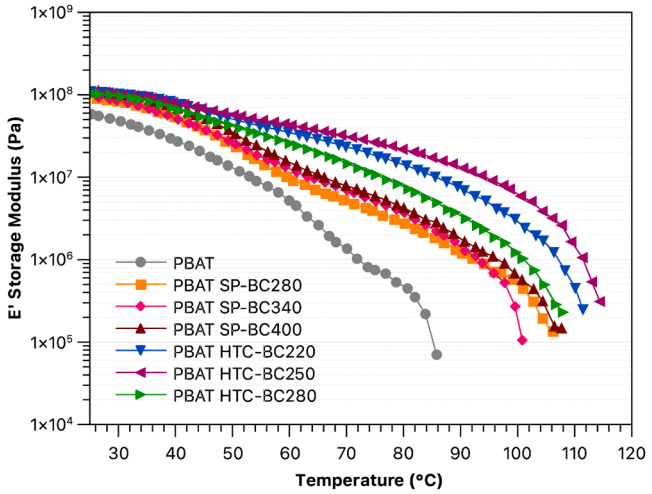

Fig. 7. Storage modulus (E') as a function of temperature of pure PBAT and all the PBAT-based bio-composites.

that the presence of both SP-BC and HTC-BC particles causes a less pronounced decrease in the peak at 1710 cm^{-1} compared to pure PBAT, and this is even more pronounced in the case of HTC-BC, see Fig. 9a–f. The formation of lateral shoulders (on the left and right) with respect to the central peak at 1710 cm^{-1} appears to be less pronounced in the presence of SP-BC, compared to pure PBAT, and slightly more pronounced in the case of HTC-BC, although the latter may be due to the fact that the peak at 1710 cm^{-1} is not significantly reduced for the PBAT/HTC-BC bio-composites.

Fig. 10a–g shows the broad bands due to the presence of hydroxyl functionalities and CH_2 symmetric and asymmetric vibrations. PBAT shows a slight increase of the hydroxyl functionalities in the first stage of exposure (*i.e.* 0–24 h) and then gradual reduction, up to disappearance, of these functionalities, see Fig. 10a. Further, the peaks assigned to the CH_2 symmetric and asymmetric vibrations disappear upon 96 h of UBV exposure in the spectrum of pure PBAT. Worth noting that PBAT SP-BC show a reduction in the content of hydroxyl groups, comparable to that of PBAT, but much less reduction in peaks due to CH_2 symmetric and asymmetric vibrations. Very interesting is the result obtained for the samples PBAT HTC-BC, a higher amplitude increases of broad peaks between 3700 and 3000 cm^{-1} is observed. In fact, the formation of free OH at 3620 cm^{-1}, hydrogen bonded OH at 3530 cm^{-1}, free OOH (or peroxide) at 3440 cm^{-1} and the broad peak at 3370 cm^{-1} are indicative of a photooxidative reaction [49]. This is due to the autocatalytic reaction, or the carboxyl terminal groups from the Norrish II reaction. Further, for the samples PBAT/HTC-BC, almost unchanged peaks due to CH_2 symmetric and asymmetric vibrations as a function of UVB exposure. Besides, the appearance of peaks/shoulders at 3410 and 3440 cm^{-1} due to autocatalytic photo-oxidation reactions can be related to the occurrence of Norrish II reaction, which leads to the formation of free OOH and/or peroxide.

To sum up, all these results suggest that the presence of both types of particles, *i.e.*, SP-BC and HTC-SP, have a protective effect by causing less cleavage of PBAT chains in bio-composites, compared to pure PBAT.

Another key parameter in assessing the photooxidation behaviour of a polymer biocomposite is to monitor the tensile properties as a function of photooxidation time.

Fig. 11 shows the dimensionless elongation at break and Young's modulus of pure PBAT, PBAT SP-BC and PBAT HTC-BC, obtained as the ratio between the values as a function of time and the value at time zero, before exposure to photooxidation.

Fig. 11a shows the dimensionless elongation at break as a function of exposure time, and this property is the main parameter normally affected by the structural and morphological changes of the polymers caused by photooxidation [55]. This graph also highlights the half time of elongation at break, a parameter evaluated as the time at which the elongation at break is half of the initial elongation. This time is considered to be the maximum time the film can be used. For pure PBAT, the half time is 17 h, whereas for PBAT SP-BC composites, the half time is reached at 72 h only if the added particles are those obtained at the

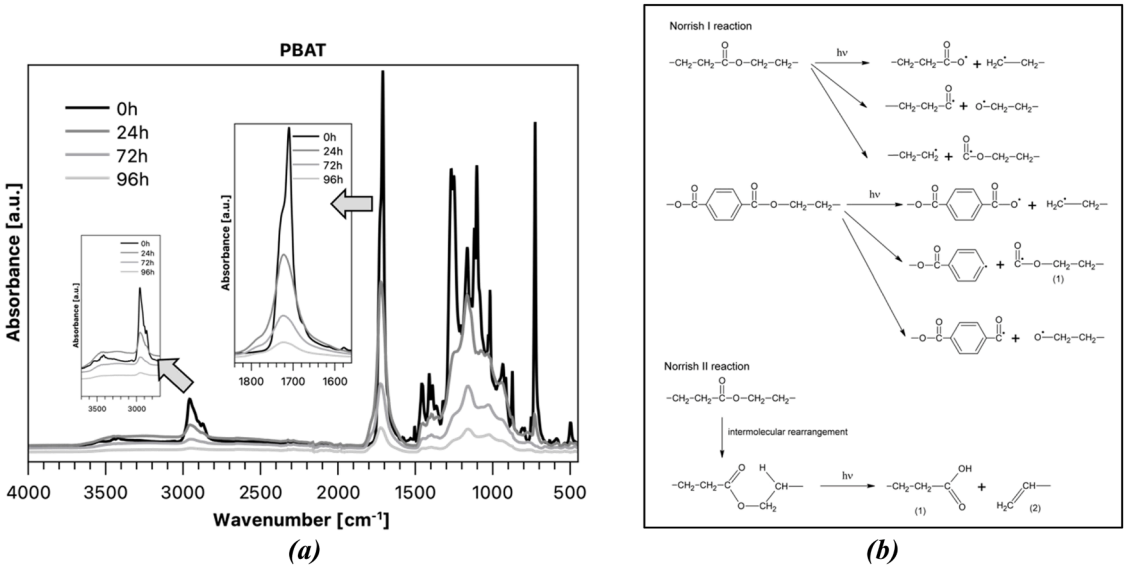

Fig. 8. (a) ATR-FTIR spectra of pure PBAT as a function of photo-oxidation time and (b) main degradation pathways for pure PBAT [49].

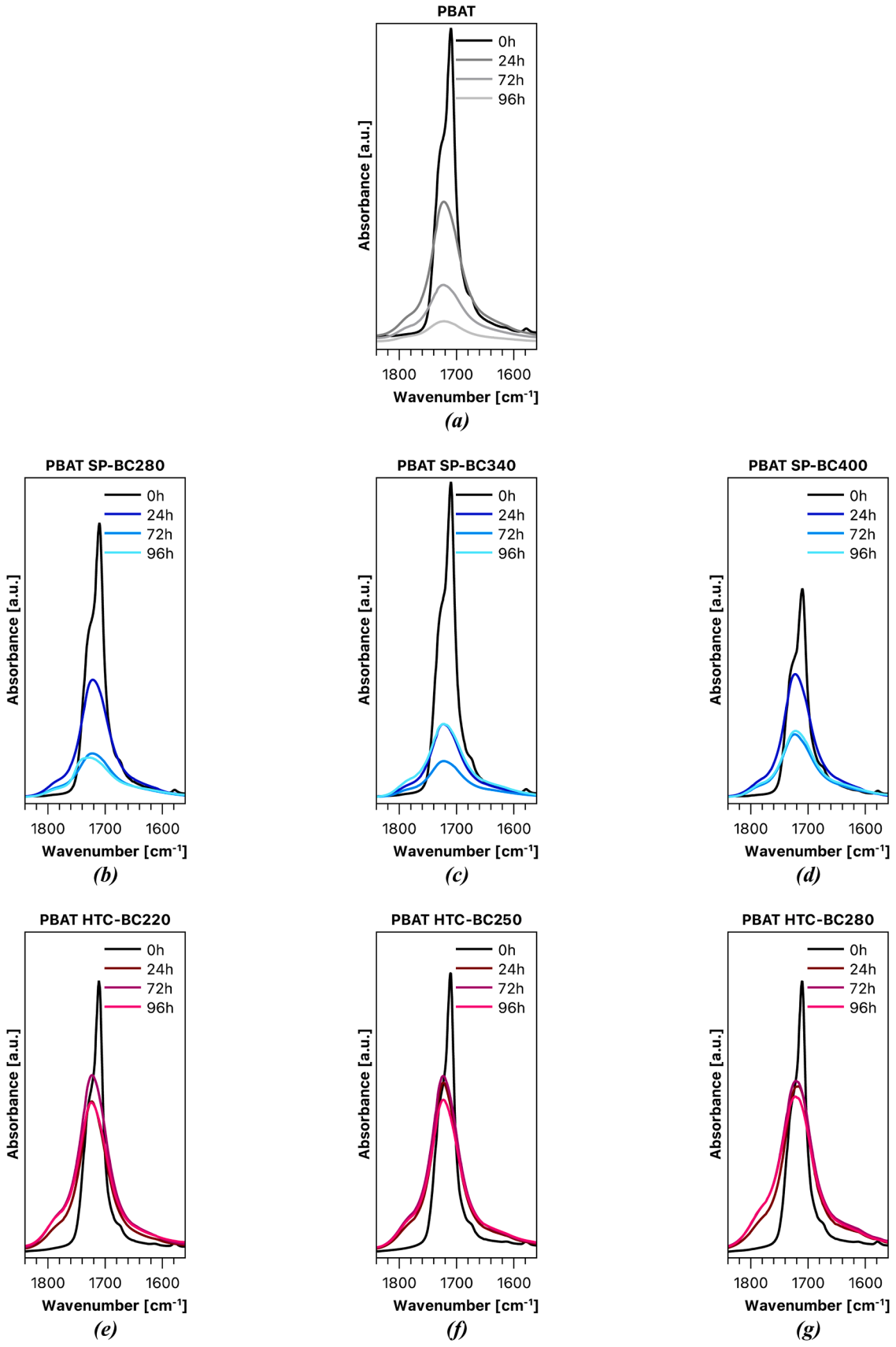

Fig. 9. The peak at 1710 $cm^{-1}$of (a) pure PBAT, (b–d) PBAT/SP-BC 280-340-400, (e–g) PBAT/HTC-BC 220-250-280 as a function of photo-oxidation time.

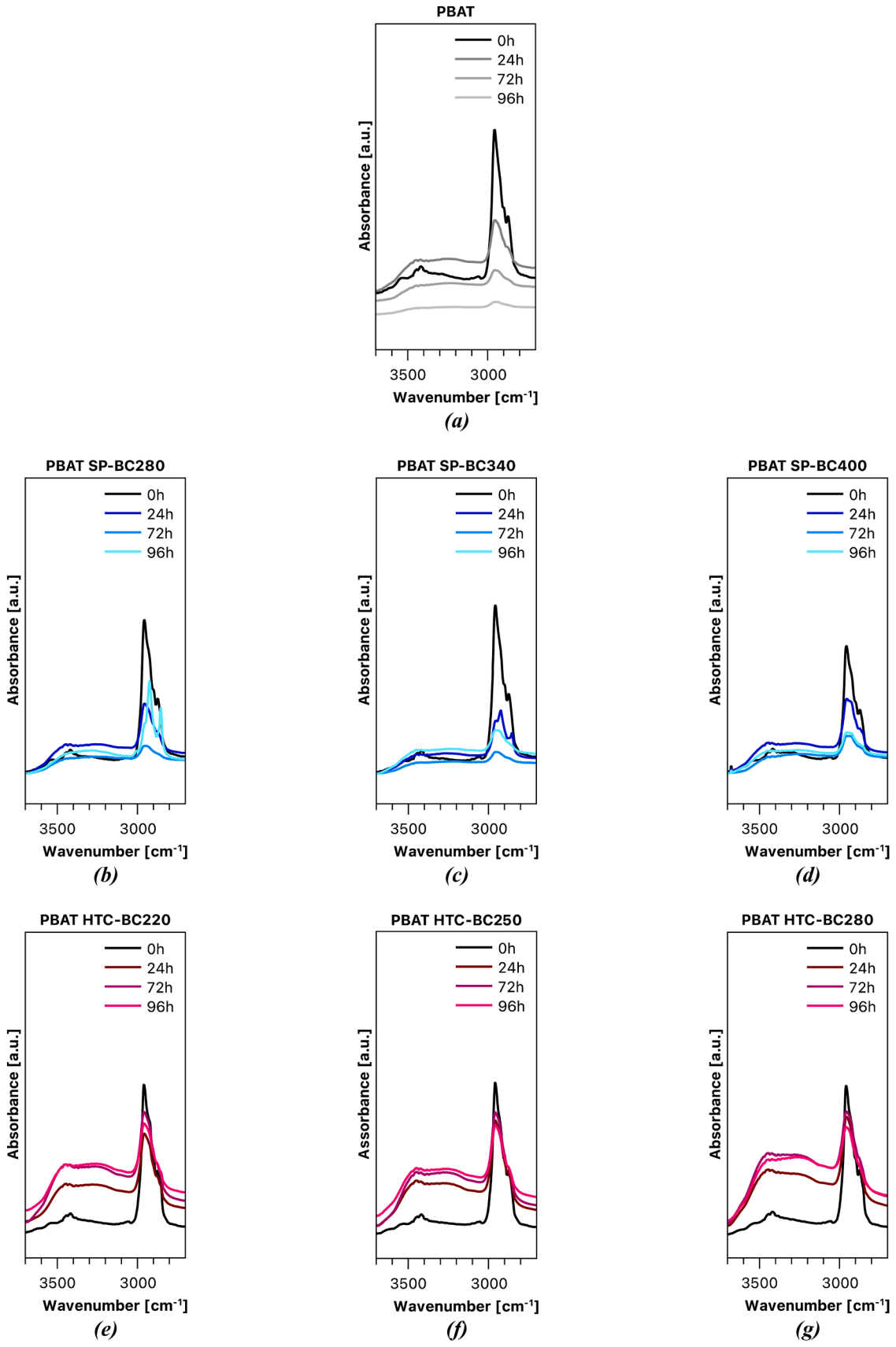

Fig. 10. Bands between 3700 and 2800 cm^{-1} of (a) pure PBAT, (b–d) PBAT/SP-BC 280-340-400, (e–g) PBAT/HTC-BC 220-250-280 as a function of photo-oxidation time.

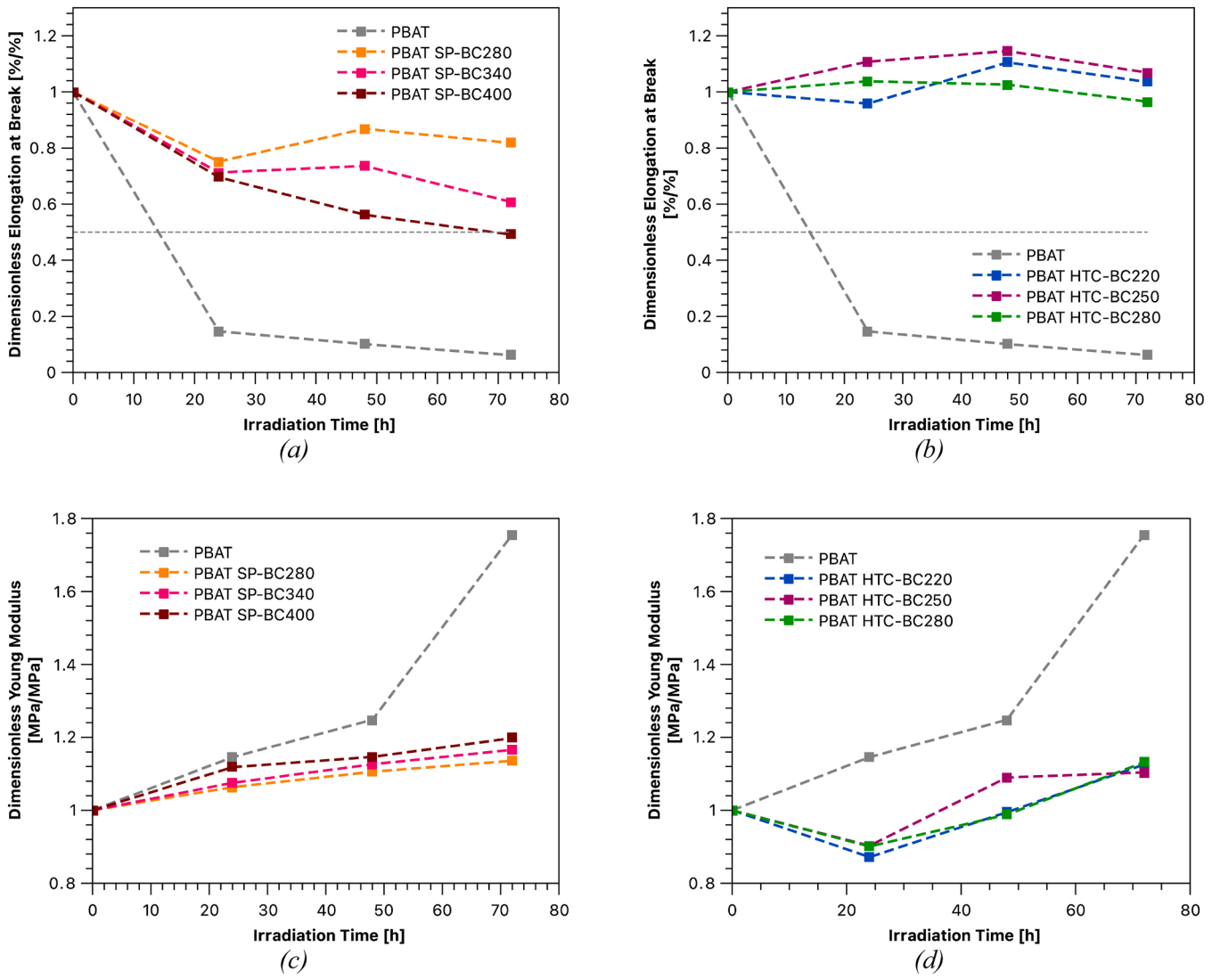

Fig. 11. (a,b) Dimensionless Elongation at Break and (c,d) Dimensionless Young Modulus of pure PBAT, PBAT/SP-BC 280-340-400 and PBAT/HTC-BC 220-250-280 as a function of photo-oxidation time.

highest pyrolysis temperature. On the contrary, for PBAT HTC-BC, the maximum time of monitoring is never reached for all the composites up to 72 h. Thus, both BC particles increase the photo-oxidation resistance of PBAT, with particular efficiency of the HTC-BC particles.

As shown in Fig. 11 the Young's modulus of pure PBAT, increases with increasing photooxidation time, as observed for semi-crystalline polymers. In the case of virgin PBAT, the increase is due to cross-linking phenomena occurring as a result of chain reactions triggered by the presence of radical oxygen. Finally, materials with ductile behaviour are involved in the brittle behaviour. In the presence of both SP-BC and HTC-BC, this behaviour is globally retarded.

To facilitate the understanding of the changes that occur in neat PBAT and PBAT-based bio-composites upon photooxidation exposure, the values of Young's modulus, tensile strength and elongation at break at different exposure times are given in Table 4. It is clear that the pure PBAT shows ductile behaviour before exposure and becomes brittle after 72 h UVB exposure. The PBAT/HTC-BC and PBAT/SP-BC samples show a brittle behaviour due to the presence of both SP-BC and HTC-BC, more pronounced for the SP-BC particles. It appears that photooxidation exposure has a limited effect on the mechanical behaviour of the

Table 4
Young Modulus (E), Tensile Strength (TS) and Elongation at Break (EB) of neat PBAT and PBAT-based bio-composites at different photooxidation times.

	Young Modulus [MPa]				Tensile Strenght [MPa]				Elongation at Break [%]			
	0h	24h	48h	72h	0h	24h	48h	72h	0h	24h	48h	72h
PBAT	41.35	40.38	50.39	60.87	9.35	10.71	11.62	16.42	562.4	82.33	56.72	34.72
PBAT SP-BC280	50.09	53.52	56.87	58.66	3.00	3.73	3.83	3.91	16.44	12.36	14.28	13.45
PBAT SP-BC340	52.24	52.35	57.66	58.25	4.08	4.72	4.90	5.13	22.34	15.92	16.44	13.60
PBAT SP-BC400	65.05	57.49	59.71	62.5	6.12	7.00	7.22	7.52	31.34	21.81	17.61	15.41
PBAT HTC-BC220	83.23	72.56	82.78	93.69	6.35	5.52	6.34	7.15	22.57	21.62	24.94	23.36
PBAT HTC-BC250	75.13	67.84	81.90	82.936	6.88	6.24	7.52	7.62	40.08	44.39	45.91	42.82
PBAT HTC-BC280	81.61	69.50	76.21	87.32	7.72	7.02	7.63	8.71	40.91	42.45	41.97	39.49

composites. Furthermore, Fig. 12 shows images of PBAT, PBAT/SP-BC280 and PBAT-HTC-BC280 films exposed to photooxidation and used for the tensile test analysis.

In order to better understand the behaviour of PBAT and PBAT-based bio-composites, solvent extraction was performed and the gel content (insoluble fraction) was evaluated. Before exposure to photooxidation (0 h), pure PBAT and all PBAT-based composites are soluble, indicating the absence of crosslinked structures. At the maximum exposure time (96 h), the samples studied show the presence of insoluble fractions and Fig. 13 shows the gel contents obtained for pure PBAT, PBAT/SP-BC and PBAT/HTC-BC bio-composites, according to the measurement and calculation reported in the experimental part. Pure PBAT shows a high gel content, approximately 51.8 %, as a natural evolution of the numerous radicals formed under UVB exposure. The presence of SP-BC in PBAT seems to reduce the gel content in the bio-composites, which also shows a slight dependence on the particle production temperatures. Specifically, as the particle production temperature increases, *i.e.* for particles containing more carbon atoms, the gel content decreases for both SP-BC and HTC-BC, although much more so for SP-BC particles. Interestingly, the presence of HTC-BC leads to the formation of significantly low gel contents, a low order of magnitude, suggesting that the presence of these particles with multiple functional surface groups interacts with PBAT and prevents the formation of cross-linked structures during photo-oxidation.

4. Conclusions

The carob waste was subjected to two different thermochemical treatments, *i.e.* slow pyrolysis (SP) and hydrothermal carbonisation (HTC), at different temperatures to produce sustainable carbon-based particles. The SP-BC and HTC-BC were then added to PBAT at 10 % by weight by melt blending to formulate sustainable composite films.

The characterisation of SP-BC and HTC-BC particles by elemental analysis (*e.g.* CHN test), spectroscopic analysis (ATR-FTIR) and morphological observations was carried out and the results suggest that both BC particles are mainly composed of carbon atoms which increase with increasing treatment temperatures, while showing low changes in hydrogen and nitrogen concentration. However, the HTC treatment leads to the production of biochar particles retaining oxygenated functional groups, as shown by the spectroscopic analysis. SEM observations of the particle surfaces show that the SP-BC have a more carbonaceous appearance, whereas the HTC-BC have a sponge-like morphology.

The rheological and mechanical characterisations of PBAT-based composites suggest that both SP-BC and HTC-BC exert a reinforcing effect on PBAT and that the polymer-filler and filler-filler interactions are more pronounced for PBAT/HTC-BC than for PBAT/SP-BC. Furthermore, the presence of both SP-BC and HTC-BC has no significantly pronounced effect on the crystallinity of PBAT.

As demonstrated, upon UVB exposure and oxygen-rich conditions, the pure PBAT shows a rapid loss of mechanical performance, becoming less ductile and hardening, and formation of high gel content, approximately 51.8 %, as a natural evolution of the numerous radicals formed under UVB exposure. Interestingly, both SP-BC and HTC-BC can slow down the photo-oxidative degradation of PBAT, thus providing protection to PBAT films, although the best results were obtained using HTC-BC. Specifically, the presence of HTC-BC leads to the maintenance of mechanical performance over the ageing period considered and the formation of significantly low gel contents, suggesting that the presence of these particles with multiple functional surface groups incentives the interactions with PBAT, preventing the formation of cross-linked structures during photo-oxidation.

CRediT authorship contribution statement

Nadka Tz. Dintcheva: Writing – review & editing, Writing – original draft, Validation, Supervision, Resources, Formal analysis, Conceptualization. **Giulia Infurna:** Writing – original draft, Validation, Methodology, Formal analysis, Data curation. **Antonio Messineo:** Validation, Supervision, Formal analysis. **Maurizio Volpe:** Writing – original draft, Validation, Supervision, Data curation, Conceptualization.

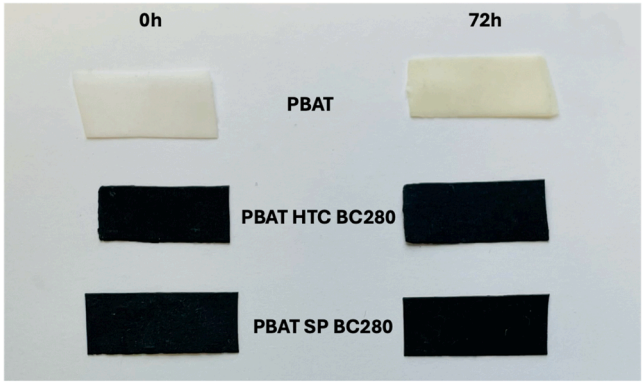

Fig. 12. Pictures of neat PBAT, PBAT/HTC280 and PBAT/SP280 before (0 h) and after UVB exposure (72 h) (*e.g.* the films used for the detection of the mechanical behaviour as a function of exposure time).

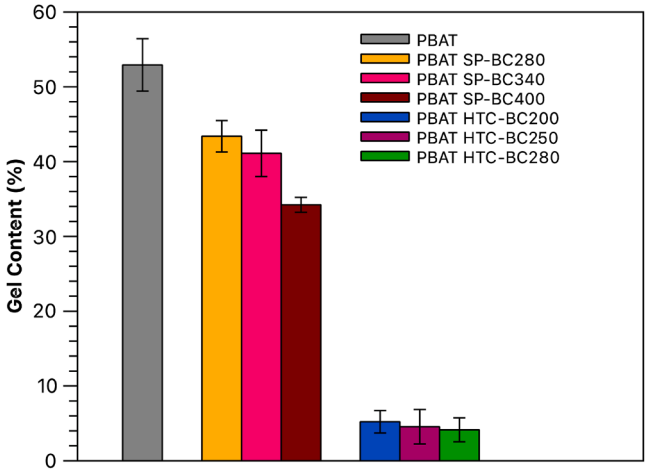

Fig. 13. The gel content of pure PBAT, PBAT/SP-BC 280-340-400 and PBAT/HTC-BC 220-250-280 at maximum photo-oxidation time (96 h).

Declaration of competing interest

The authors declare that they have no known competing financial interests or personal relationships that could have appeared to influence the work reported in this paper.

Acknowledgments

This study was carried out within the MICS (Made in Italy - Circular and Sustainable) Extended Partnership and received funding from the European Union Next-Generation EU (Piano Nazionale di Ripresa e Resilienza (PNRR) - Missione 4 Componente 2, Investimento 1.3 - D.D. 1551.11-10-2022, PE00000004). This manuscript reflects only the authors' views and opinions, neither the European Union nor the European Commission can be considered responsible for them.

Supplementary materials

Supplementary material associated with this article can be found, in the online version, at doi:10.1016/j.polymdegradstab.2025.111224.

Data availability

Data will be made available on request.

References

[1] EU Commission European Green Deal 2019.
[2] European Commission Communication From The Commission To The European Parliament, The Council, The European Economic And Social Committee And The Committee Of The Regions Closing the loop -an EU action plan for the circular economy; Brussels, 2018.
[3] A. Di Bartolo, G. Infurna, N.T. Dintcheva, A review of bioplastics and their adoption in the circular economy, Polymers 13 (2021), https://doi.org/10.3390/polym13081229.
[4] P.R. Yaashikaa, P.S. Kumar, S. Varjani, A. Saravanan, A critical review on the biochar production techniques, characterization, stability and applications for circular bioeconomy, Biotechnol. Rep. 28 (2020), https://doi.org/10.1016/j.btre.2020.e00570.
[5] M. Maniscalco, G. Infurna, G. Caputo, L. Botta, N.T. Dintcheva, Slow pyrolysis as a method for biochar production from carob waste: process investigation and products' characterization, Energies 14 (2021), https://doi.org/10.3390/en14248457.
[6] M. Volpe, D. Panno, R. Volpe, A. Messineo, Upgrade of citrus waste as a biofuel via slow pyrolysis, J. Anal. Appl. Pyrolysis 115 (2015) 66–76, https://doi.org/10.1016/j.jaap.2015.06.015.
[7] X. Shi, J. Wang, A comparative investigation into the formation behaviors of char, liquids and gases during pyrolysis of pinewood and lignocellulosic components, Bioresour. Technol. 170 (2014) 262–269, https://doi.org/10.1016/j.biortech.2014.07.110.
[8] B. Sizirici, Y.H. Fseha, I. Yildiz, T. Delclos, A. Khaleel, The effect of pyrolysis temperature and feedstock on date palm waste derived biochar to remove single and multi-metals in aqueous solutions, Sustain. Environ. Res. 31 (2021), https://doi.org/10.1186/s42834-021-00083-x.
[9] S. Al Arni, Comparison of slow and fast pyrolysis for converting biomass into fuel, Renew. Energy 124 (2018) 197–201, https://doi.org/10.1016/j.renene.2017.04.060.
[10] M. Ahmad, S.S. Lee, X. Dou, D. Mohan, J.-K. Sung, J.E. Yang, Y.S. Ok, Effects of pyrolysis temperature on soybean stover- and peanut shell-derived biochar properties and TCE adsorption in water, Bioresour. Technol. 118 (2012) 536–544, https://doi.org/10.1016/j.biortech.2012.05.042.
[11] K.B. Cantrell, P.G. Hunt, M. Uchimiya, J.M. Novak, K.S. Ro, Impact of pyrolysis temperature and manure source on physicochemical characteristics of biochar, Bioresour. Technol. 107 (2012) 419–428, https://doi.org/10.1016/j.biortech.2011.11.084.
[12] M. Giorcelli, P. Savi, A. Khan, A. Tagliaferro, Analysis of biochar with different pyrolysis temperatures used as filler in epoxy resin composites, Biomass Bioenergy 122 (2019) 466–471, https://doi.org/10.1016/j.biombioe.2019.01.007.
[13] A. Tomczyk, Z. Sokołowska, P. Boguta, Biochar physicochemical properties: pyrolysis temperature and feedstock kind effects, Rev. Environ. Sci. Biotechnol. 19 (2020) 191–215, https://doi.org/10.1007/s11157-020-09523-3.
[14] G. Infurna, G. Caruso, N.T.Z. Dintcheva, Sustainable materials containing biochar particles: a review, Polymers 15 (2023) 343, https://doi.org/10.3390/polym15020343.
[15] M. Uchimiya, L.H. Wartelle, K.T. Klasson, C.A. Fortier, I.M. Lima, Influence of pyrolysis temperature on biochar property and function as a heavy metal sorbent in soil, J. Agric. Food Chem. 59 (2011) 2501–2510, https://doi.org/10.1021/jf104206c.
[16] W.T. Tsai, R. Ayestas, C.H. Tsai, Y.Q. Lin, Preparation and characterization of porous materials from pineapple peel at elevated pyrolysis temperatures, Materials 15 (2022), https://doi.org/10.3390/ma15134686.
[17] I.F. Titiladunayo, A.G. McDonald, O.P. Fapetu, Effect of temperature on biochar product yield from selected lignocellulosic biomass in a pyrolysis process, Waste Biomass Valorization 3 (2012) 311–318, https://doi.org/10.1007/s12649-012-9118-6.
[18] Y. Sun, B. Gao, Y. Yao, J. Fang, M. Zhang, Y. Zhou, H. Chen, L. Yang, Effects of feedstock type, production method, and pyrolysis temperature on biochar and hydrochar properties, Chem. Eng. J. 240 (2014) 574–578, https://doi.org/10.1016/j.cej.2013.10.081.
[19] D. Bona, M. Lucian, D. Feretti, S. Silvestri, I. Zerbini, F. Merzari, A. Messineo, M. Volpe, Phytotoxicity and genotoxicity of agro-industrial digested sludge hydrochar: the role of heavy metals, Sci. Total Environ. 871 (2023) 162138, https://doi.org/10.1016/j.scitotenv.2023.162138.
[20] J.L. Goldfarb, A.H. Hubble, Q. Ma, M. Volpe, G. Severini, G. Andreottola, L. Fiori, Valorization of cow manure via hydrothermal carbonization for phosphorus recovery and adsorbents for water treatment, J. Environ. Manag. 308 (2022) 114561, https://doi.org/10.1016/j.jenvman.2022.114561.
[21] S. Mia, B. Singh, F.A. Dijkstra, Aged biochar affects gross nitrogen mineralization and recovery: A ^{15} N study in two contrasting soils, GCB Bioenergy 9 (2017) 1196–1206, https://doi.org/10.1111/gcbb.12430.
[22] J.W. Lee, M. Kidder, B.R. Evans, S. Paik, A.C. Buchanan Iii, C.T. Garten, R. C. Brown, Characterization of biochars produced from cornstovers for soil amendment, Environ. Sci. Technol. 44 (2010) 7970–7974, https://doi.org/10.1021/es101337x.
[23] Y. Ding, Y. Liu, S. Liu, Z. Li, X. Tan, X. Huang, G. Zeng, L. Zhou, B. Zheng, Biochar to improve soil fertility. A review, Agron. Sustain. Dev. (2016) 36, https://doi.org/10.1007/s13593-016-0372-z.
[24] Y. Lin, P. Munroe, S. Joseph, R. Henderson, A. Ziolkowski, Water extractable organic carbon in untreated and chemical treated biochars, Chemosphere 87 (2012) 151–157, https://doi.org/10.1016/j.chemosphere.2011.12.007.
[25] M.B. Ahmed, J.L. Zhou, H.H. Ngo, W. Guo, M. Chen, Progress in the preparation and application of modified biochar for improved contaminant removal from water and wastewater, Bioresour. Technol. 214 (2016) 836–851, https://doi.org/10.1016/j.biortech.2016.05.057.
[26] M. Barbalini, M. Bartoli, A. Tagliaferro, G. Malucelli, Phytic acid and biochar: an effective all bio-sourced flame retardant formulation for cotton fabrics, Polymers 12 (2020) 811, https://doi.org/10.3390/polym12040811.
[27] M.R. Ribeiro, Y. De Moraes Guimarães, I.F. Silva, C.A. Almeida, M.S.V. Silva, M. A. Nascimento, U.P. Da Silva, E.V. Varejão, N. Dos Santos Renato, A.P.D. C. Teixeira, et al., Synthesis of value-added materials from the sewage sludge of cosmetics industry effluent treatment plant, J. Environ. Chem. Eng. 9 (2021) 105367, https://doi.org/10.1016/j.jece.2021.105367.
[28] S. Fang, L. Zhao, G. Rong, B. Chen, X. Xu, H. Qiu, X. Cao, Converting coastal silt into subgrade soil with biochar as reinforcing agent, CO_2 adsorbent, and carbon sequestrating material, J. Environ. Manag. 344 (2023) 118394, https://doi.org/10.1016/j.jenvman.2023.118394.
[29] C. Guizani, F. Javier, E. Sanz, S. Salvador, C. Guizani, F.J. Escudero Sanz, S. Salvador, Influence of temperature and particle size on the single and mixed atmosphere gasification of biomass char with H_2O and CO_2 influence of temperature and particle size on the single and mixed atmosphere gasification of biomass char with H_2O and CO_2, Fuel Process. Technol. 134 (2015) 175–188, https://doi.org/10.1016/j.fuproc.2015.01.031ï.
[30] M. Karimi, M. Shirzad, J.A.C. Silva, A.E. Rodrigues, Biomass/biochar carbon materials for CO_2 capture and sequestration by cyclic adsorption processes: a review and prospects for future directions, J. CO2 Util. 57 (2022) 101890, https://doi.org/10.1016/j.jcou.2022.101890.
[31] L. Grande, I. Pedroarena, S.A. Korili, A. Gil, Hydrothermal liquefaction of biomass as one of the most promising alternatives for the synthesis of advanced liquid biofuels: a review, Materials 14 (2021), https://doi.org/10.3390/ma14185286.
[32] M. Hitzl, A. Corma, F. Pomares, M. Renz, The hydrothermal carbonization (HTC) plant as a decentral biorefinery for wet biomass, Catal. Today 257 (2015) 154–159, https://doi.org/10.1016/j.cattod.2014.09.024.
[33] C. Ye, Hydrochar as an environment-friendly additive to improve the performance of biodegradable plastics, Sci. Total Environ. (2022).
[34] M.T. Reza, J. Andert, B. Wirth, D. Busch, J. Pielert, J.G. Lynam, J. Mumme, Hydrothermal carbonization of biomass for energy and crop production, Appl. Bioenergy 1 (2014), https://doi.org/10.2478/apbi-2014-0001.
[35] H.S. Kambo, A. Dutta, A comparative review of biochar and hydrochar in terms of production, physico-chemical properties and applications, Renew. Sustain. Energy Rev. 45 (2015) 359–378, https://doi.org/10.1016/j.rser.2015.01.050.
[36] A. Kruse, N. Dahmen, Water – a magic solvent for biomass conversion, J. Supercrit. Fluids 96 (2015) 36–45, https://doi.org/10.1016/j.supflu.2014.09.038.
[37] M. Lucian, F. Merzari, M. Gubert, A. Messineo, M. Volpe, Industrial-scale hydrothermal carbonization of agro-industrial digested sludge: filterability enhancement and phosphorus recovery, Sustainability 13 (2021) 9343, https://doi.org/10.3390/su13169343.
[38] G. Infurna, L. Botta, M. Maniscalco, E. Morici, G. Caputo, S. Marullo, F. D'Anna, N. T.Z. Dintcheva, Biochar particles obtained from agricultural carob waste as a suitable filler for sustainable biocomposite formulations, Polymers 14 (2022) 3075, https://doi.org/10.3390/polym14153075.
[39] G. Infurna, L. Botta, I. Ingargiola, M. Maniscalco, G. Caputo, N.T.Z. Dintcheva, Biochar from digestate pyrolysis as a filler for biopolymer blends: effect of blend composition, J. Polym. Environ. (2023), https://doi.org/10.1007/s10924-023-03108-1.
[40] R. Herrera, L. Franco, A. Rodríguez-Galán, J. Puiggalí, Characterization and degradation behavior of poly(Butylene adipate-co-terephthalate)s, J. Polym. Sci. Part A Polym. Chem. 40 (2002) 4141–4157, https://doi.org/10.1002/pola.10501.
[41] M. Volpe, A. Messineo, M. Mäkelä, M.R. Barr, R. Volpe, C. Corrado, L. Fiori, Reactivity of cellulose during hydrothermal carbonization of lignocellulosic biomass, Fuel Process. Technol. 206 (2020) 106456, https://doi.org/10.1016/j.fuproc.2020.106456.
[42] M. Mäkelä, M. Volpe, R. Volpe, L. Fiori, O. Dahl, Spatially resolved spectral determination of polysaccharides in hydrothermally carbonized biomass, Green Chem. 20 (2018) 1114–1120, https://doi.org/10.1039/C7GC03676K.
[43] M.T. Reza, W. Yan, M.H. Uddin, J.G. Lynam, S.K. Hoekman, C.J. Coronella, V. R. Vásquez, Reaction kinetics of hydrothermal carbonization of loblolly pine, Bioresour. Technol. 139 (2013) 161–169, https://doi.org/10.1016/j.biortech.2013.04.028.
[44] Z. Liu, Z. Wang, H. Chen, T. Cai, Z. Liu, Hydrochar and pyrochar for sorption of pollutants in wastewater and exhaust gas: a critical review, Environ. Pollut. 268 (2021) 115910, https://doi.org/10.1016/j.envpol.2020.115910.
[45] M. Volpe, L. Fiori, R. Volpe, A. Messineo, Upgrading of olive tree trimmings residue as biofuel by hydrothermal carbonization and torrefaction: a comparative study, Chem. Eng. Trans. 50 (2016) 13–18, https://doi.org/10.3303/CET1650003.
[46] M. Volpe, L. Fiori, From olive waste to solid biofuel through hydrothermal carbonisation: the role of temperature and solid load on secondary char formation and hydrochar energy properties, J. Anal. Appl. Pyrolysis 124 (2017) 63–72, https://doi.org/10.1016/j.jaap.2017.02.022.
[47] N.T.Z. Dintcheva, R. Arrigo, S. Carroccio, G. Curcuruto, M. Guenzi, C. Gambarotti, G Filippone, Multi-functional polyhedral oligomeric silsesquioxane-functionalized

carbon nanotubes for photo-oxidative stable ultra-high molecular weight polyethylene-based nanocomposites, Eur. Polym. J. 75 (2016) 525–537, https://doi.org/10.1016/j.eurpolymj.2016.01.002.
[48] Y. Wang, C. Xu, D. Wu, W. Xie, K. Wang, Q. Xia, H. Yang, Rheology of the cellulose nanocrystals filled poly(ε-caprolactone) biocomposites, Polymer 140 (2018) 167–178, https://doi.org/10.1016/j.polymer.2018.02.050 (Guildf).
[49] T. Kijchavengkul, R. Auras, M. Rubino, E. Alvarado, J.R. Camacho Montero, J. M. Rosales, Atmospheric and soil degradation of aliphatic-aromatic polyester films, Polym. Degrad. Stab. 95 (2010) 99–107, https://doi.org/10.1016/j.polymdegradstab.2009.11.048.
[50] R. Qi, D.L. Jones, Q. Liu, Q. Liu, Z. Li, C. Yan, Field test on the biodegradation of poly(Butylene adipate-co-terephthalate) based mulch films in soil, Polym. Test. 93 (2021) 107009, https://doi.org/10.1016/j.polymertesting.2020.107009.
[51] S. Mohanty, S.K. Nayak, Biodegradable nanocomposites of poly (Butylene Adipate-Co-terephthalate) (PBAT) with organically modified nanoclays, Int. J. Plast. Technol. 14 (2010) 192–212, https://doi.org/10.1007/s12588-010-0018-y.
[52] Y. Cai, J. Lv, J. Feng, Spectral characterization of four kinds of biodegradable plastics: poly (Lactic acid), poly (Butylenes adipate-Co-terephthalate), poly (Hydroxybutyrate-Co-hydroxyvalerate) and poly (Butylenes succinate) with FTIR and Raman spectroscopy, J. Polym. Environ. 21 (2013) 108–114, https://doi.org/10.1007/s10924-012-0534-2.
[53] H.M. Elkholy, S.S. Hamdani, M.O. Alghaysh, I. Wyman, E. Duncan, Y. Wang, K. Li, M. Rabnawaz, Design of carboxylic acid-functionalized poly(Butylene adipate- *Co* -Terephthalate) for recyclable and biodegradable zero-waste paper packaging, Adv. Sustain. Syst. (2024) 2400621, https://doi.org/10.1002/adsu.202400621.
[54] X. Meng, Y. Ye, R. Yang, Computational and experimental study on the mechanism of CO_2 production during photo-oxidative degradation of poly(butylene adipate-co-terephthalate): differences between PBA and PBT segments, Macromolecules 56 (2023) 7749–7762, https://doi.org/10.1021/acs.macromol.3c01649.
[55] L. Botta, N.T.Z. Dintcheva, F.P. La Mantia, The role of organoclay and matrix type in photo-oxidation of polyolefin/clay nanocomposite films, Polym. Degrad. Stab. 94 (2009) 712–718, https://doi.org/10.1016/j.polymdegradstab.2008.12.017.